



ELSEVIER

Available online at www.sciencedirect.com

SCIENCE @ DIRECT®

Deep-Sea Research I 52 (2005) 259–278

DEEP-SEA RESEARCH
PART I

www.elsevier.com/locate/dsr

A regime diagram for classifying turbulent large eddies in the upper ocean

Ming Li^{a,*}, Chris Garrett^b, Eric Skillingstad^c

^aHorn Point Lab, University of Maryland Center for Environmental Science, P.O. Box 775, Cambridge, MA 21613, USA

^bDepartment of Physics and Astronomy, University of Victoria, P.O. Box 3055, Victoria, BC, Canada V8W 2Y2

^cCollege of Oceanic and Atmospheric Sciences, Oregon State University, 104 Ocean Admin Bldg, Corvallis, OR 97331, USA

Received 26 January 2004; accepted 17 September 2004

Available online 15 December 2004

Abstract

A large eddy simulation (LES) model is used to examine how buoyancy-driven thermal convection, wind-driven shear turbulence and wind/wave-driven Langmuir circulation compete to generate turbulence in the ocean surface mixed layer. The turbulent Langmuir number La_t , a ratio of friction velocity to surface Stokes drift velocity, and the Hoenikker number Ho , a ratio of buoyancy forcing to wave forcing, are two controlling dimensionless parameters. We explore low-order turbulence statistics in the La_t and Ho parameter space for a wide range of atmospheric forcing conditions and construct a regime diagram to differentiate buoyancy-, shear- and wave-driven turbulence. All three types of turbulent flows are anisotropic but show different orderings of turbulence intensities: vertical > (downwind, crosswind) in convective turbulence; downwind > crosswind > vertical in shear turbulence; crosswind \approx vertical > downwind in Langmuir turbulence. These orderings of turbulence intensities can be explained by examining the turbulence energy production in three directions. Buoyancy production in the vertical direction dominates turbulence generation in convective turbulence, whereas shear production in the downwind direction dominates turbulence generation in shear-driven turbulence. In Langmuir turbulence, however, Stokes production due to surface waves generates turbulence energy in both crosswind and vertical directions.

Turbulence in the wind-driven upper ocean shows a transition from shear to Langmuir turbulence as La_t decreases. A fully-developed sea state corresponds to $La_t \approx 0.3$ and lies within the Langmuir regime. Vertical turbulence intensity in Langmuir turbulence is about two times larger than that in shear turbulence and falls into the range observed in the upper ocean. Hence the wind-driven upper ocean will be dominated by Langmuir turbulence under typical sea state conditions. Transition from Langmuir to convective turbulence occurs around $Ho = O(1)$, which is much greater than $Ho = O(0.01)$ obtained using typical heat fluxes and wind speeds.

© 2004 Elsevier Ltd. All rights reserved.

Keywords: Ocean mixed layer; Turbulence; Langmuir circulation; Convection; Shear; Numerical model

*Corresponding author. Tel.: +1 410 221 8420; fax: +1 410 221 8490.

E-mail address: mingli@hpl.umces.edu (M. Li).

1. Introduction

The upper region of the ocean typically exhibits a surface mixed layer having nearly uniform density structure. Turbulent large eddies are generated by surface fluxes of buoyancy and momentum and by surface waves, and are thought to contribute to turbulent mixing in the upper ocean. Thermal convection can be generated when the ocean loses heat through longwave radiation or evaporative cooling. Convective eddies typically form polygonal patterns with narrow cold plumes descending around the edges of an upwelling polygon. The shear generated in wind-driven currents can produce Kelvin–Helmholtz billows with their axes oriented roughly at right angles to the shear. The interaction between the mean particle (Stokes) drift of surface waves and the wind-driven shear current produces Langmuir circulation, consisting of counter-rotating vortices with their axes roughly parallel to the wind direction (Langmuir, 1938). Individually, these turbulent eddies have been subject to intensive investigations (e.g. Lombardo and Gregg, 1989; Weller and Price, 1988). Under realistic conditions, the upper ocean is forced by a combination of wind stress, wave forcing and surface heat fluxes. All three types of turbulent flows may co-exist. It is therefore important to investigate these large eddies from a common framework.

A large eddy simulation (LES) model has been developed to investigate turbulent large eddies in the upper ocean. The model is forced by wind stress and surface heat flux at the ocean surface and by a vortex force term representing the time-averaged effect of surface waves. The LES model thus provides a common modeling framework to simulate different types of turbulent eddies and combinations of different turbulence types. Skyllingstad and Denbo (1995, hereafter SD) used LES to simulate Langmuir circulation and convection in the surface mixed layer. They carried out numerical experiments with different combinations of wind stress, wave forcing and convective forcing. SD found that the buoyancy force is typically less powerful than the vortex force (wave forcing) in generating mixing, in apparent agreement with a previous study using a 2D model

(Li and Garrett, 1995, hereafter LG95). McWilliams et al. (1997, hereafter MSM) investigated turbulent dynamics in a rotating surface boundary layer. In particular, they carried out a detailed comparison of turbulence statistics and characteristics between shear turbulence and Langmuir turbulence. MSM found that turbulent vertical fluxes of momentum and heat are greatly enhanced by the presence of wave forcing due to the Stokes drift current. Recent LES simulations by Skyllingstad et al. (1999, 2000) have focussed on comparing turbulence statistics with upper-ocean observations such as microstructure measurements. There have also been interesting studies to incorporate wave effects into K-profile mixed-layer parameterization by using LES simulation results (McWilliams and Sullivan, 2001; Smyth et al., 2002). Noh et al. (2004) have recently studied the combined effects of wave breaking and Langmuir circulation in a LES model of the upper ocean.

These modeling investigations have demonstrated that LES models are capable of realistically simulating turbulent flows in the upper ocean. The upper ocean is forced by a great variety of atmospheric conditions, including a wide range of wind speeds, different sea state conditions, and buoyancy forcing conditions ranging from day-time heating to night-time cooling. However, there have been relatively few modeling explorations of the wide-range forcing conditions. SD carried out a limited number of case studies to compare wave forcing with buoyancy forcing. Skyllingstad (2001) examined how the crosswind velocity in Langmuir circulation varies with the friction velocity and Stokes drift current. Neither of these two studies has led to a comprehensive summary of turbulent flow regimes in the ocean mixed layer. Moreover, most LES results are analysed in dimensional units. A number of model input parameters are required to specify various forcing terms in the LES model. Without model nondimensionalization, it is difficult to know if two LES runs are dynamically equivalent. The only exception is the paper by MSM who defined a turbulent Langmuir number to compare the role of surface waves to wind stress, but MSM limited their study to a comparison between two LES runs, one representative of shear turbulence and the other

representative of Langmuir turbulence. We need to continue this line of approach and explore LES results in nondimensional parameter space. How do the turbulence characteristics change as we vary the turbulent Langmuir number from shear forced to Langmuir forced conditions? The same analysis should be extended to include the effects of surface heat fluxes. LG95 defined a dimensionless Hoenikker number to compare convective forcing with wave forcing (i.e. vortex force) driving Langmuir circulation, but they employed a 2D model with constant viscosity and diffusivity. It is necessary to re-examine the results using a 3D LES model which can realistically simulate the three-dimensional structure of convective eddies.

In this paper, we shall focus on the dynamics of turbulent large eddies in a well-mixed surface layer. We shall not consider the effects of pre-existing stratification nor pre-existing currents which may result from previous wind events. We begin with a density (temperature) distribution that is uniform in a surface mixed layer but has a sharp gradient in the thermocline below. In this model setup, turbulence eddies could not overcome the strong stratification force at the base of the mixed layer and do not cause entrainment into the stratified thermocline. We shall carry out systematic modeling of large eddies and examine how thermal convection, shear turbulence and Langmuir circulation compete to generate turbulence. The plan for this paper is as follows. In Section 2, we nondimensionalize the LES equations and identify controlling dimensionless parameters. In Section 3, we examine the transition from shear to Langmuir turbulence, and in Section 4 the transition from Langmuir to convective turbulence. In Section 5, we summarize results in the parameter space and interpret different orderings of turbulence intensities by using turbulence kinetic energy equations. In the conclusion section, we will summarize the main results and discuss the plan for future research.

2. Model nondimensionalization

An LES model is based upon a filtering of the fundamental fluid equations of motion. MSM

obtained the filtered Craik–Leibovich equations in a rotating oceanic surface boundary layer as follows:

$$\begin{aligned} \frac{\partial \tilde{\mathbf{v}}}{\partial \tilde{t}} + \tilde{\mathbf{v}} \cdot \nabla \tilde{\mathbf{v}} + f \hat{\mathbf{z}} \times (\tilde{\mathbf{v}} + \tilde{\mathbf{u}}_s) \\ = -\frac{1}{\rho_0} \nabla \tilde{\pi} + \alpha g \tilde{\theta} \hat{\mathbf{z}} + \tilde{\mathbf{u}}_s \times \tilde{\boldsymbol{\omega}} + \text{SGS}, \end{aligned} \quad (1)$$

$$\frac{\partial \tilde{\theta}}{\partial \tilde{t}} + (\tilde{\mathbf{v}} + \tilde{\mathbf{u}}_s) \cdot \nabla \tilde{\theta} = \text{SGS}, \quad (2)$$

$$\nabla \cdot \tilde{\mathbf{v}} = 0, \quad (3)$$

where f is the Coriolis parameter, $\tilde{\mathbf{v}}$ the velocity vector, $\tilde{\boldsymbol{\omega}}$ the vorticity vector, $\tilde{\theta}$ temperature, $\tilde{\mathbf{u}}_s$ Stokes drift, $\tilde{\pi}$ modified pressure. These equations include the augmentation of LES Navier–Stokes equations by a generalized vortex force, $\mathbf{u}_s \times (f \hat{\mathbf{z}} + \boldsymbol{\omega})$, and an additional advection of any material property P by the wave-induced Lagrangian motion, $\mathbf{u}_s \cdot \nabla P$. The subgrid-scale terms as presented by SGS are only shown schematically in the above equations.

We shall start from a surface mixed layer with uniform density distribution and investigate how thermal convection, shear flow and Langmuir circulation compete to generate turbulence. The LES model is forced by wind stress and surface heat flux at the ocean surface. We nondimensionalize distance, velocities, time, pressure and temperature as

$$\tilde{\mathbf{v}} = u_* \mathbf{v}, \quad \tilde{\mathbf{u}}_s = U_s \mathbf{u}_s, \quad (4)$$

$$\tilde{\mathbf{x}} = \mathbf{x} / \beta, \quad (5)$$

$$\tilde{t} = t / (\beta u_*), \quad (6)$$

$$\tilde{\pi} = \rho_0 u_*^2 \pi, \quad (7)$$

$$\tilde{\theta} = \frac{Q}{C_p \rho u_*} \theta, \quad (8)$$

where u_* is the water friction velocity, U_s and $1/\beta$ are the surface velocity and the e-folding depth of the Stokes drift current, ρ_0 a reference water density, C_p the specific heat at constant pressure and Q the net surface heat flux. After substituting

(4)–(8) into (1)–(3), we obtain

$$\begin{aligned} \frac{\partial \mathbf{v}}{\partial t} + \mathbf{v} \cdot \nabla \mathbf{v} + \frac{1}{Ro} \hat{\mathbf{z}} \times (\mathbf{v} + La_t^{-2} \mathbf{u}_s) \\ = -\nabla \pi + La_t^{-2} \left[-\frac{1}{4} Ho \theta \hat{\mathbf{z}} + \mathbf{u}_s \times \tilde{\boldsymbol{\omega}} \right] + \text{SGS}, \end{aligned} \quad (9)$$

$$\frac{\partial \tilde{\theta}}{\partial t} + (\mathbf{v} + La_t^{-2} \mathbf{u}_s) \cdot \nabla \tilde{\theta} = \text{SGS}, \quad (10)$$

$$\nabla \cdot \mathbf{v} = 0. \quad (11)$$

With this choice of nondimensionalization, no dimensionless parameters appear in the boundary conditions.

There are three dimensionless parameters in this set of nondimensionalized equations. The first parameter is the turbulent Langmuir number as defined by MSM

$$La_t = \left(\frac{u_*}{U_s} \right)^{1/2}, \quad (12)$$

which is the ratio of the water friction velocity to the surface Stokes drift velocity. A wind-driven upper ocean without surface waves corresponds to $La_t = \infty$. The second parameter is the Hoennikker number, as defined by LG95,

$$Ho = \frac{4B_0}{U_s \beta u_*^2}, \quad (13)$$

where $B_0 = -\alpha g Q / (\rho_w C_p)$ is the surface buoyancy flux. It compares the unstable buoyancy force driving thermal convection with the vortex force (wave forcing) driving Langmuir circulation. The third parameter $Ro = u_* \beta / f$ is the Rossby number. The Hoennikker number Ho and turbulent Langmuir number La_t are two controlling parameters. At $Ho = 0$, La_t describes the transition from shear turbulence to Langmuir turbulence in a wind-driven upper ocean. At a given value of La_t , positive (negative) Ho describes the effects of destabilizing (stabilizing) surface buoyancy flux on turbulence dynamics in the ocean mixed layer. Although the Coriolis force affects the turning of mean currents, the eddy turnover time of upper-ocean large eddies is typically much shorter than the inertial period. The parameter Ro is thus expected to play a

secondary role. We shall discuss the effects of rotation when we analyse turbulence statistics later.

To investigate turbulence dynamics numerically, we shall use the LES model which was first developed by Skillingstad and Denbo (1995), hereafter and later improved for various mixed-layer simulations (e.g. Skillingstad et al., 1999, 2000). We note that the Stokes Coriolis force missing in SD has now been taken into account. Readers are referred to Skillingstad et al. (1999) for more details on the numerical scheme. We choose a model domain with a horizontal dimension of $120 \times 120 \text{ m}^2$ and a vertical dimension of 50 m at a resolution of 1 m. We also run the model with a large domain size of $240 \times 240 \times 50 \text{ m}^3$ but at a coarser resolution of 2 m. The model is initialized with a homogeneous density layer down to 40 m depth, followed by linearly stratified water with a thickness of 10 m and a buoyancy frequency $N = 0.02 \text{ s}^{-1}$. Hence the model has an additional dimensionless parameter βH , which is a ratio of the mixed layer depth H to the e-folding depth of the Stokes drift current. This ratio is typically large. Because the vortex force associated with the Stokes drift of surface waves is concentrated near the ocean surface, we argue that turbulence dynamics in the mixed-layer should be relatively independent of βH at large values of βH (see also Li and Garrett, 1997). However, this parameter could become important in a shallow mixed layer or in shallow-water coastal oceans or lakes.

For oceanic applications, we will run the LES model in dimensional units but we will analyse the model results in nondimensionalized space. In order to cover the two-dimensional $Ho-La_t$ parameter space, we will first explore LES results along some line transects in this space. In Section 3, we ignore the effect of surface heat flux ($Ho = 0$) and examine turbulence dynamics as we vary La_t . In Section 4, we fix La_t but vary Ho by changing surface heat flux. By carefully exploring the parameter space, we shall construct a regime diagram in $Ho-La_t$ space that can differentiate shear-, wave- and buoyancy-driven turbulence over a wide range of atmospheric forcing conditions.

3. Transition from shear to Langmuir turbulence

If waves were absent at the ocean surface, wind-driven turbulent flows in the ocean surface boundary layer would have the characteristics of shear-driven turbulence as found in a wall boundary layer. When wind blows over the ocean surface, it generates currents as well as surface waves. The interaction between the waves and currents produces Langmuir circulation/turbulence that differs from shear-driven turbulence. To quantify how surface waves modify turbulence dynamics in the ocean mixed layer, MSM carried out a detailed comparison of low-order turbulence statistics between shear turbulence ($La_t = \infty$) and typical Langmuir turbulence ($La_t = 0.3$). They found that Langmuir turbulence has more uniform mean velocity, greater anisotropy, enhanced velocity variances and skewness, and larger energy dissipation, compared with shear turbulence without the effects of surface waves.

There are a wide variety of sea states in the wind-driven upper ocean, ranging from fully-developed seas to fetch-limited conditions. The size of waves is governed not only by local wind speed, but also by the fetch over which the wind blows. Adding to this complexity, large swell generated at a remote ocean site may arrive at the local region of interest. Even in fully developed seas, surface waves consist of a range of sizes only describable by a wave spectrum. When calculating the Stokes drift current, we need to consider the contribution from all wave components. Thus the Stokes drift at the sea surface will not be simply proportional to the wind speed and La_t can take a range of values. Furthermore, the vertical profile of the Stokes drift current may be different from the exponential profile. Kenyon (1969) and Huang (1971) calculated the Stokes drift current for random surface waves by using directional wave spectrum. In a 2D model of Langmuir circulation, Li and Garrett (1993) used an approximation to this Stokes drift profile but found that the model results did not differ much from those obtained using the exponential profile. Hence we shall use the exponential profile to represent the Stokes drift current in this paper. In this profile, a prescription of the surface drift and e-folding depth completely

determines the vertical profile of the Stokes drift current. The e-folding depth will be fixed to 4.77 m (i.e. $\beta H = 8.4$) in most of our runs but the surface drift will be varied over a wide range in order to vary La_t .

As MSM have already provided a fairly detailed comparison of all low-order turbulence statistics between typical shear and Langmuir turbulence, we shall focus on changes in three components of turbulence intensities as La_t is varied between the two types of turbulence. Before examining turbulence statistics, we look at the time evolution of turbulence field in a LES run with dimensionless parameters $La_t = 0.34$ and $Ho = 0$. The LES model not only resolves the mean flow but also energy-containing turbulent large eddies. At any instant we define the mean velocity to be the horizontal average of the velocity field. Turbulent velocities are departures from this horizontal average. In Fig. 1 we plot time series of three velocity variances (turbulence intensities) averaged over the mixed layer depth. The time is scaled by $1/(\beta u_*)$ which is related to the turnover time of near-surface eddies generated by the vortex force of surface waves, assuming a velocity scale of u_* and a depth scale of $1/\beta$. After a spin-up period of $\beta u_* t \approx 35$, the turbulence intensities settle down to nearly constant values. Turbulence statistics will be calculated using the turbulence fields obtained during this quasi-equilibrium period. Our choice for model integration time is in accordance with MSM who found that turbulence reaches a quasi-equilibrium over a period of $O(1/f) = 3$ h where $f = 10^{-4} \text{ s}^{-1}$. If the LES model is run over many inertial periods, the depth-integrated volume transport will be consistent with that calculated from a steady Ekman–Stokes current (see MSM). This would require long integration times. Moreover, turbulence in the surface mixed layer may cause entrainment from the stratified flow below. Since our focus is on turbulence dynamics in the mixed layer, we run the LES model until turbulence reaches the quasi-equilibrium state and low-order turbulence statistics do not change with time.

In Fig. 2 we compare turbulence statistics between three LES runs at $Ho = 0$: Case 1 with $La_t = 0.34$ typical of Langmuir turbulence, Case 2

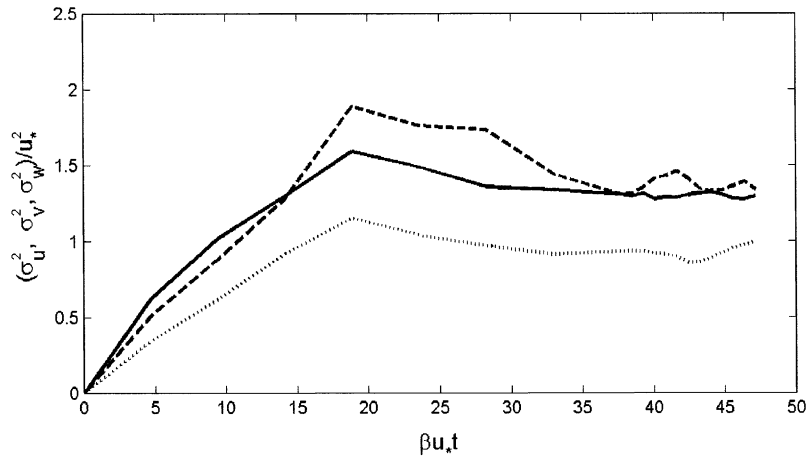


Fig. 1. Time series of downwind (dotted), crosswind (dashed) and vertical (solid) velocity variances obtained from a LES run with $La_t = 0.34$ and $Ho = 0$.

with $La_t = 10$ typical of shear turbulence and Case 3 with $La_t = 0.73$ representative of an intermediate type. The vertical profiles of three velocity variances reveal significant differences. As La_t is reduced, the downwind velocity variance decreases, whereas the crosswind and vertical velocity variances increase. Most noticeably, the vertical velocity variance is significantly larger at $La_t = 0.34$ than at $La_t = 0.73$ and 10 (see Fig. 2c). As shown in Fig. 2d, momentum fluxes all show a linear decay with depth, consistent with a quasi-equilibrium state. Figs. 2e and f show profiles of the mean downwind and crosswind velocities. Both exhibit less shear as La_t is reduced, showing a more effective vertical momentum transfer as we move from shear to Langmuir turbulence.

Due to the effect of the Coriolis force, the horizontal current continues to be deflected to the right, as shown in a vertical profile of the mean crosswind current in Fig. 2f. Although Langmuir turbulence generates vigorous mixing which homogenizes the downwind velocity, the crosswind velocity remains slightly sheared inside the mixed layer. The same result was reported in MSM. We suspect that this apparent difference in the mean current may be a manifestation of a time-dependent effect. Our model integration time is much longer than the eddy turnover time, but it is still shorter than the inertial period. It is possible that the mean crosswind wind will become

homogeneous if our model is integrated over many inertial periods. However, turbulence statistics presented in Figs. 2a–d are insensitive to the effect of rotation. In fact, turbulence statistics were obtained from an averaging period of $(37–47)/\beta u_*$ in Case 1 but from a much later period of $(75–94)/\beta u_*$ in Cases 2 and 3. Although the Coriolis force affects the turning of the mean current, the turbulence statistics can be obtained over a time scale shorter than the inertial period, as long as the model integration time is much longer than the eddy turnover time.

As a result of more effective turbulent momentum transport within the mixed layer, large shear develops near the mixed-layer base (see Figs. 2e and f) and can potentially lead to shear instability and entrainment from the thermocline below. In the model runs shown in this paper, we have selected an initial temperature profile with strong stratification in the thermocline region. The surface mixed-layer did not penetrate from the stratified thermocline, even though some large eddies clearly reach the base of the mixed layer. Analysis of the mean velocity and temperature profiles confirms that the gradient Richardson number stays above the critical threshold of $\frac{1}{4}$ near the mixed-layer base where large shear has developed.

Turbulence intensities measured in the wind-driven upper ocean show a large departure from shear turbulence. Using a neutrally-buoyant

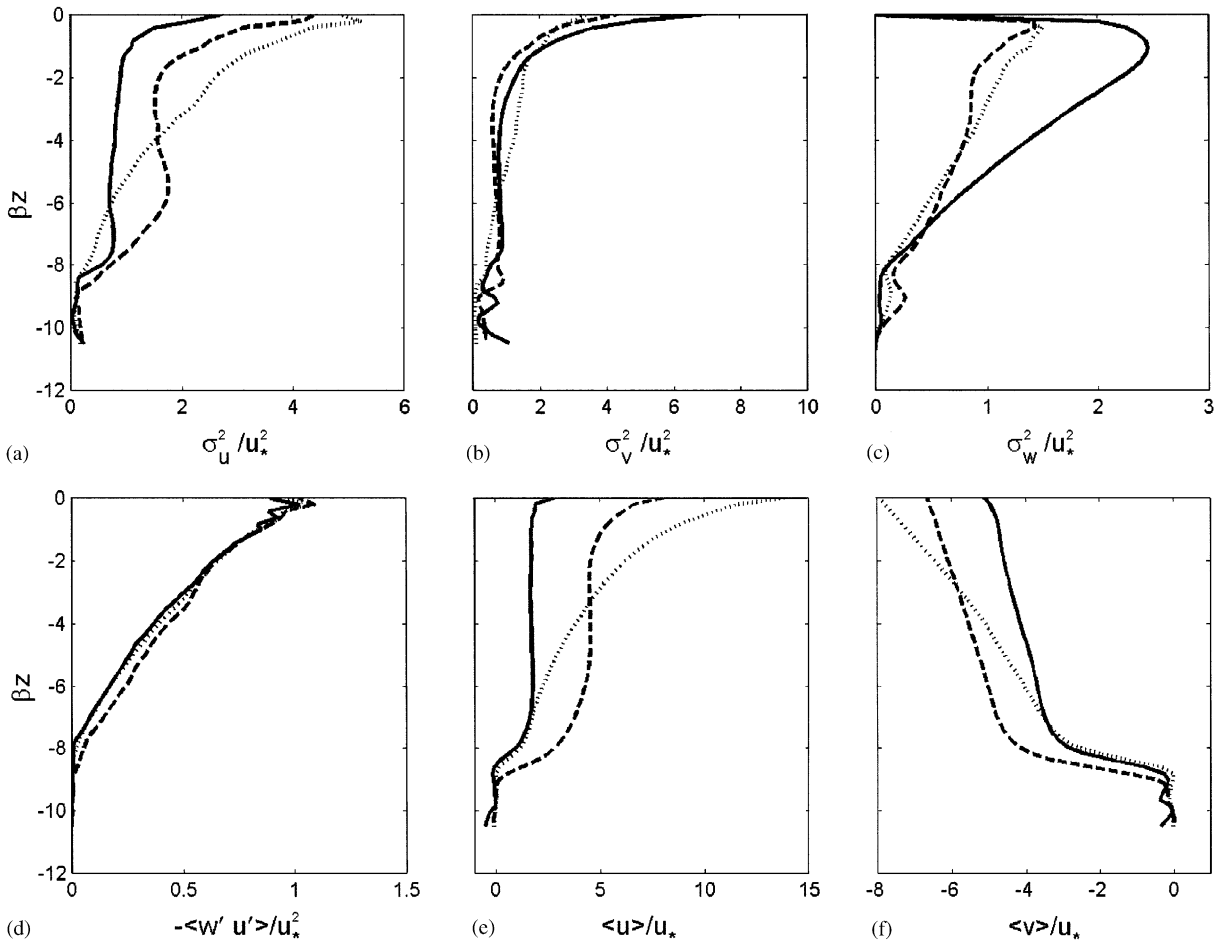


Fig. 2. Comparison of turbulence statistics between three LES runs with $La_t = 10$ (dotted), 0.73 (dashed) and 0.34 (solid) but all at $Ho = 0$. Vertical profiles of velocity variance in downwind (a), crosswind (b) and vertical (c) directions. Vertical profiles of momentum flux (d), mean velocity in downwind (e) and crosswind (f) directions.

Lagrangian float to follow water parcels, D’Asaro (2001) obtained estimates of vertical velocity at different depths in the ocean mixed layer. The resulting vertical profile of vertical turbulence intensity σ_w^2/u_*^2 (corrected for measurement errors) has a maximum of about 2 at a depth of $-0.2H$ (mixed-layer depth). This compares with a maximum of about 1 in profiles of σ_w^2/u_*^2 obtained from laboratory experiments of zero-pressure-gradient boundary layers over smooth and rough walls. We reproduce D’Asaro’s results in Fig. 3b. For comparison, we also plot the vertical profiles of σ_w^2/u_*^2 calculated from the LES model with $La_t = 0.34$ and ∞ in Fig. 3a. In agreement with

the upper-ocean measurements, vertical turbulence intensity in Langmuir turbulence is twice as much as that in shear turbulence. Thus Langmuir circulation is likely responsible for generating turbulence observed in the upper ocean. We note that a surface boundary layer driven by wind stress is not exactly the same as a wall boundary layer driven by an external flow over a non-slip solid boundary. Near the boundary, there are clear differences in σ_w^2/u_*^2 between the shear turbulence simulated by the model and the laboratory experiments.

A key characteristic of turbulent flows in the ocean mixed layer is the magnitude of the vertical

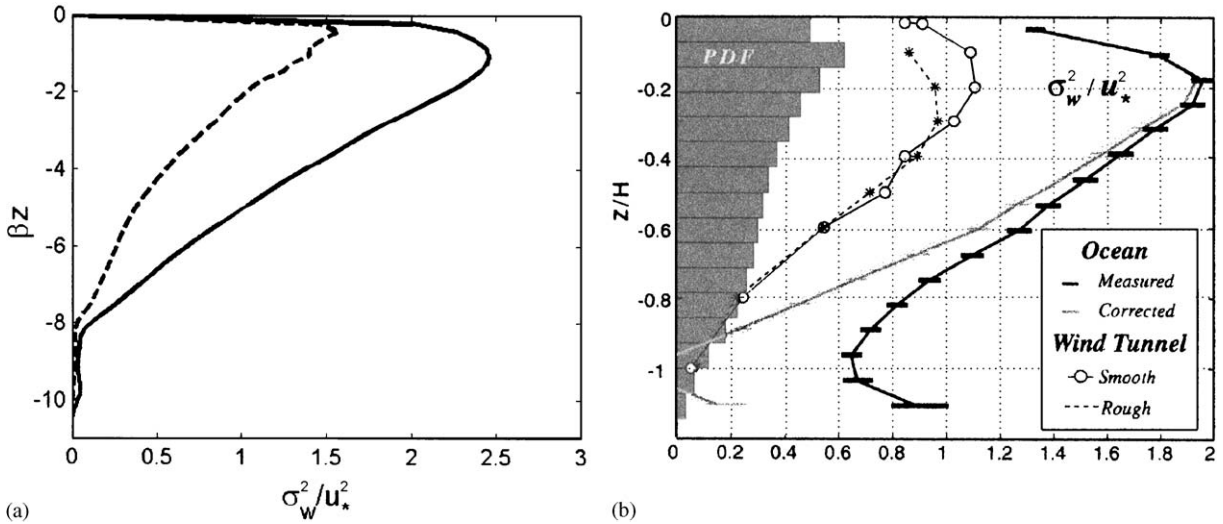


Fig. 3. Comparison between vertical profiles of vertical velocity variance between LES model (a) and observations (b). In (a), the solid line corresponds to Langmuir turbulence with $La_t = 0.34$, whereas the dashed line to shear turbulence with $La_t = \infty$. In (b), data points indicated by circles and stars were obtained in a smooth and rough wall boundary layer, whereas the black line was obtained from measurements of a neutrally-buoyant float in the upper ocean and the grey line includes correction for measurement biases (from D’Asaro, 2001).

velocity. The larger the vertical velocity, the more effective vertical transports of momentum and scalars will be. Since the vertical velocity has a zero mean, vertical velocity variance $\overline{\sigma_w^2}$ averaged over the mixed layer depth provides a good measure of turbulence intensity in the vertical direction. We have considered $1/\beta$ (or a multiple of this value) as a possible depth scale to average $\overline{\sigma_w^2}$ in Langmuir turbulence, but some turbulent eddies penetrate to the bottom of the mixed layer. Hence the mixed layer depth appears to be the more appropriate length scale for averaging the turbulence intensity. In Fig. 4, we show how $\overline{\sigma_w^2}$ normalized by u_*^2 varies with turbulent Langmuir number La_t . As La_t decreases, $\overline{\sigma_w^2}/u_*^2$ changes little until La_t falls to about 0.7. It rises rapidly with further decreases in La_t . Fig. 4 suggests a separation between two turbulence regimes with a dividing line located at $La_t \approx 0.7$. On the right of this line turbulence is dominated by shear production and vertical turbulence intensity can be approximately scaled by the friction velocity such that the ratio $\overline{\sigma_w^2}/u_*^2$ is nearly constant. As shown in Fig. 5, turbulence intensities in this regime show an ordering of

downwind > crosswind > vertical component. This is consistent with shear-forced turbulence where shear production generates turbulence energy in the downwind direction, which is then redistributed to the crosswind and downwind components by pressure and turbulence transport terms. To the left of the dividing line lies Langmuir turbulence where the turbulence intensity cannot be scaled by the friction velocity alone. Vertical velocity variance $\overline{\sigma_w^2}/u_*^2$ exceeds that of shear turbulence and increases rapidly as La_t decreases. As wave forcing gets stronger, turbulence intensity gets larger. Examination of three velocity variances reveal an ordering of crosswind \approx vertical > downwind components, as shown in Fig. 5. In this Langmuir regime, turbulence production by the Stokes drift injects energy directly to the crosswind and vertical components, while the shear production in the downwind direction is reduced because of a more uniform mean flow.

Results presented in Fig. 4 can be put into the context of upper-ocean observations. The depth-averaged vertical velocity variance $\overline{\sigma_w^2}/u_*^2$ is approximately 0.7 in the shear regime but varies

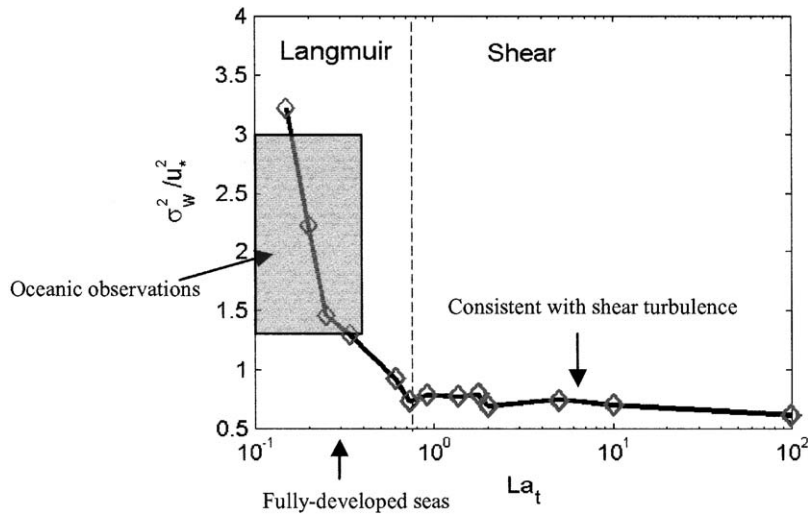


Fig. 4. The depth-averaged vertical velocity variance as a function of La_t at $Ho = 0$, showing a transition from shear to Langmuir turbulence. When $La_t > 0.7$, the normalized vertical velocity variance is nearly constant so that turbulence intensity is scaled by the friction velocity only. When $La_t < 0.7$, the normalized vertical velocity variance increases rapidly with decreasing La_t , showing additional turbulence generation due to the Stokes drift. The shaded grey box indicates the range of vertical velocity variances observed in the upper ocean while a fully-developed sea corresponds to $La_t \approx 0.3$.

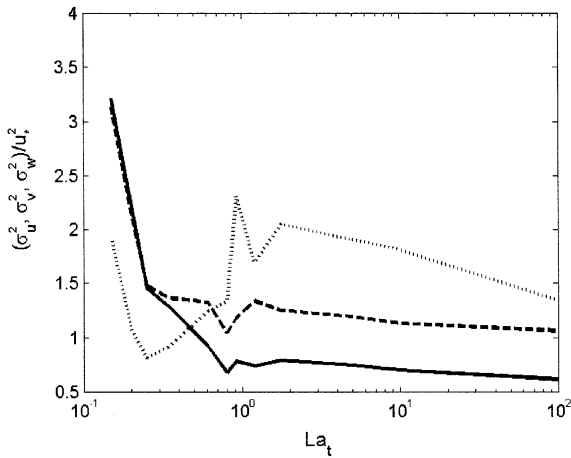


Fig. 5. Depth-averaged velocity variances in three directions (dotted for downwind, dashed for crosswind and solid for vertical) as a function of La_t at $Ho = 0$. In Langmuir turbulence, $\sigma_w^2 \approx \sigma_u^2 > \sigma_v^2$. In shear turbulence, we have an ordering of $\sigma_u^2 > \sigma_v^2 > \sigma_w^2$.

between 1 and 3 in the Langmuir regime. Turbulence measurements obtained from Lagrangian floats gave a range (1.5–3.0) in the Strait of Georgia (D’Asaro and Dairiki, 1997) and 1.35 in

the open-ocean North Pacific (D’Asaro, 2001). Comparison between these observations and LES results suggests that turbulence in the wind-driven upper ocean falls into the Langmuir regime. Assuming fully-developed seas and using the empirical Pierson and Moskowitz wave spectrum modified for directional spreading, Li and Garrett (1993) obtained a ratio of the surface Stokes drift to the water friction velocity in the range of 9.2–13.8. This translates to a range of $La_t = (0.27–0.33)$, which falls into the Langmuir regime shown in Fig. 4. If the Stokes drift current is stronger because of swell or other wave components not considered in the Pierson and Moskowitz wave spectrum, La_t , may be smaller. In developing seas or fetch-limited conditions, the Stokes drift current may be weaker, consequently the turbulent Langmuir number would be larger and one moves towards the shear turbulence regime. According to Fig. 4, $\overline{\sigma_w^2}/u_*^2$ should be smaller in fetch-limited conditions than in fully-developed seas. However, $\overline{\sigma_w^2}/u_*^2$ was found in a range (1.5–3.0) in the Strait of Georgia (D’Asaro and Dairiki, 1997), which is up to a factor of 2 larger than 1.35 observed in the open-ocean North

Pacific (D'Asaro, 2001). This seems to contradict the LES results shown in Fig. 4. At present we do not have a clear explanation for this discrepancy. To have a definitive comparison between the LES results and the float observations, however, we may need to run LES simulations driven by the actual forcing recorded during the observational periods.

One possible cause for the discrepancy might be that the vertical decay scale of the Stokes drift current may be different between the fetch-limited coastal ocean and the fully-developed open ocean.

To explore this, we have conducted two additional runs of Langmuir turbulence ($La_t = 0.34$) with the e-folding depth at 2.4 and 9.6 m. Fig. 6 shows a comparison of low-order turbulence statistics between the three runs with the depth ratio $\beta H = 4.2, 8.4$ and 16.7 . Quite surprisingly, this depth ratio has a significant effect on the mean currents in both downwind and crosswind directions. However, its effect on the velocity variances in the two horizontal directions is minimal. The depth of the maximum vertical velocity variance appears to scale with the e-folding depth of the

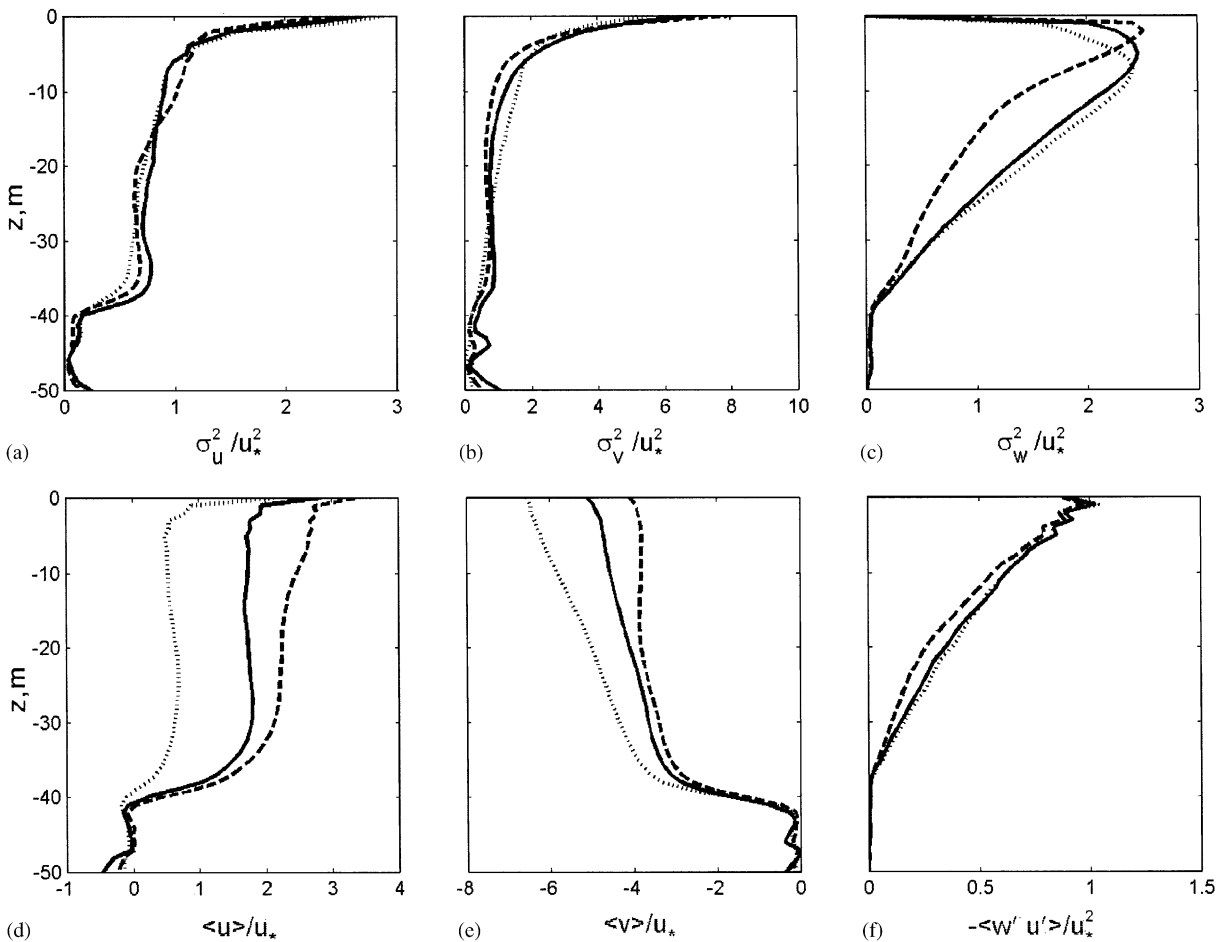


Fig. 6. Comparison of turbulence statistics between three LES runs of Langmuir turbulence ($La_t = 0.34$ and $Ho = 0$) using different e-folding depths of the Stokes drift current: $\beta H = 4.2$ (dotted), 8.4 (solid) and 16.7 (dashed). Vertical profiles of velocity variance in downwind (a), crosswind (b) and vertical (c) directions. Vertical profiles of momentum flux (d), mean velocity in downwind (e) and crosswind (f) directions.

Stokes drift current and varies inversely with βH . The depth-averaged $\overline{\sigma_w^2}/u_*^2$ at $\beta H = 16.7$ is about 25% less than that at $\beta H = 4.2$ and 8.4. This difference is significant and requires us to be careful when using Fig. 4 to interpret observations. However, it cannot explain a factor of two difference in vertical turbulence intensity observed between coastal and open ocean conditions.

4. Transition from Langmuir/shear to convective turbulence

We have explored the transition from shear to Langmuir turbulence in a wind-driven upper ocean. How will turbulence statistics and characteristic change if the ocean is losing or gaining heat at the surface? Under what heat flux conditions will turbulence be driven primarily by unstable buoyancy force rather than mechanical forces associated with wind and surface waves? Using a 2D model with constant eddy viscosity (and diffusivity) and assuming no variability in the wind direction, LG95 examined the transition from Langmuir to convective turbulence in an initially-homogeneous mixed layer. They found that buoyancy forcing due to surface heat loss is much weaker than wave forcing under typical oceanic conditions. From numerical solutions and scale analysis, LG95 showed that the transition value Ho_c must be as large as about 3 in order for convective forcing to be comparable to wave forcing at high Reynolds number limit. However, Ho_c is reduced as eddy viscosity increases and approaches zero when the viscous force is large enough to suppress the generation of Langmuir circulation (see LG95). If small eddies resolved in the LES model produced a large effective eddy viscosity, the transition value Ho_c may be comparable to typical values of $Ho = O(10^{-2})$ found in the ocean. Another concern about LG95's 2D results is that convective eddies form polygonal or roll (in the presence of shear) patterns and are inherently three-dimensional. Using a 3D LES model, SD compared two model runs of Langmuir circulation: one without surface heat flux ($Ho = 0$) and one with a heat loss rate of -160 W m^{-2} ($Ho = 0.06$). They found that wave forcing dom-

inates thermal forcing near the surface and partially confirmed LG95 results, but convective eddies penetrate deeper and dominate turbulence dynamics at lower depths. To fully understand the transition from Langmuir to convective turbulence, we need to explore a range of Ho values.

We carry out a number of LES runs at a fixed value of $La_t = 0.34$. We examine both heating and cooling cases so that Ho takes both negative and positive values. Fig. 7 compares three LES runs. Case 1 with $Ho = 0$ represents Langmuir turbulence without surface heat flux (neutral). It corresponds to a wind speed of 10 m s^{-1} and a surface Stokes drift of about 0.1 m s^{-1} . Case 2 with $Ho = 0.083$ corresponds to a surface heat loss rate of 200 W m^{-2} (unstable) while Case 3 with $Ho = -0.25$ corresponds to a surface heating rate of 600 W m^{-2} (stable). As shown in Figs. 7c and d, surface heating inhibits vertical penetration of turbulent eddies whereas surface cooling promotes vertical penetration. In particular, the addition of an unstable buoyancy force to Langmuir turbulence leads to a much deeper profile of $\overline{\sigma_w^2}/u_*^2$, as turbulent eddies are able to penetrate deeper into the mixed layer. Vertical profiles of the mean downwind and crosswind velocities are about the same between the neutral and unstable cases (case 1 and case 2), but surface heating (case 3) has led to a more rapid decay of the mean current with depth (Figs. 7e and f). As shown in Fig. 7g, the mean temperature in both heating and cooling cases is barely changed from the initial profile during the model integration period. The heat flux in the cooling case (Case 2) shows a typical overshoot near the mixed-layer base, whereas the heat flux in the heating case (Case 3) shows a simple decay with depth (Fig. 7h).

To investigate the transition from Langmuir to convective turbulence, we examine how three depth-averaged velocity variances ($\overline{\sigma_u^2}/u_*^2$, $\overline{\sigma_v^2}/u_*^2$, $\overline{\sigma_w^2}/u_*^2$) vary with Ho in Fig. 8. At small values of Ho , crosswind and vertical turbulence intensities are about the same, but both are much larger than the downwind component, as found in Langmuir turbulence. As Ho increases and more buoyancy force is added, all three components of turbulence intensities increase. At $Ho = 0.8$, the vertical velocity variance $\overline{\sigma_w^2}/u_*^2$ is twice as much as that

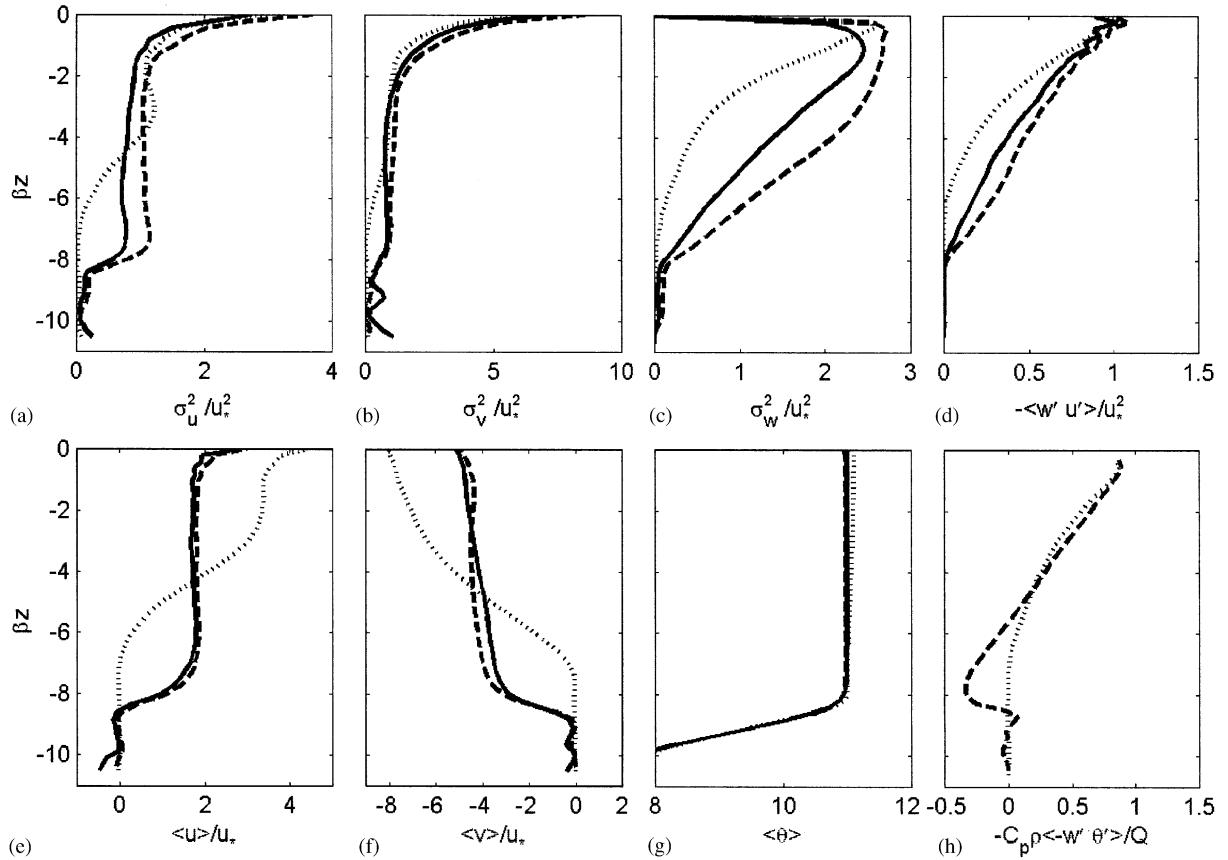


Fig. 7. Turbulence statistics for three values of Ho (dotted for -0.25 , dashed for 0.083 and solid for 0) but at a fixed value of $La_t = 0.34$. Vertical profiles of velocity variance in downwind (a), crosswind (b) and vertical (c) directions, momentum flux (d), mean velocity in downwind (e) and crosswind (f) directions, mean temperature (g) and heat flux (h).

at $Ho = 0$. At this point, wave forcing and buoyancy forcing contribute equally to the vertical turbulence intensity. Coincidentally, for $Ho > 0.8$, the ordering of turbulence intensity switches to vertical > crosswind > downwind components. At large values of Ho , the vertical turbulence intensity exceeds the two horizontal components (of similar magnitude), as expected in convective turbulence. If we compare the LES results with the previous 2D results from LG95, the doubling of root-mean-square (rms) vertical velocity (or quadrupling of σ_w^2 / u_*^2) actually occurs around $Ho = 3$, in a surprising agreement with the LG95 scaling result. However, as we show later in Fig. 13, this threshold value of Ho_c changes with La_t . Nonetheless, the threshold Hoenniker number, at which

Langmuir circulation and thermal convection contribute equally to the turbulence generation in the mixed layer, occurs at order of 1, which is much greater than the values of 10^{-2} found in typical oceanic conditions.

At large values of Ho , turbulence is in the convective regime. An appropriate scale for convective turbulence is Deardorff's convective velocity scale $w_* = (B_0 H)^{1/3}$, where B_0 is the surface buoyancy flux and H is the mixed layer depth. We have scaled the three components of turbulence intensities using w_*^2 in Fig. 9. As expected, the normalized turbulence intensities approach constant levels for $Ho > 10$. At small values of Ho , the turbulence bears the characteristics of Langmuir turbulence and greatly exceeds the convective scale.

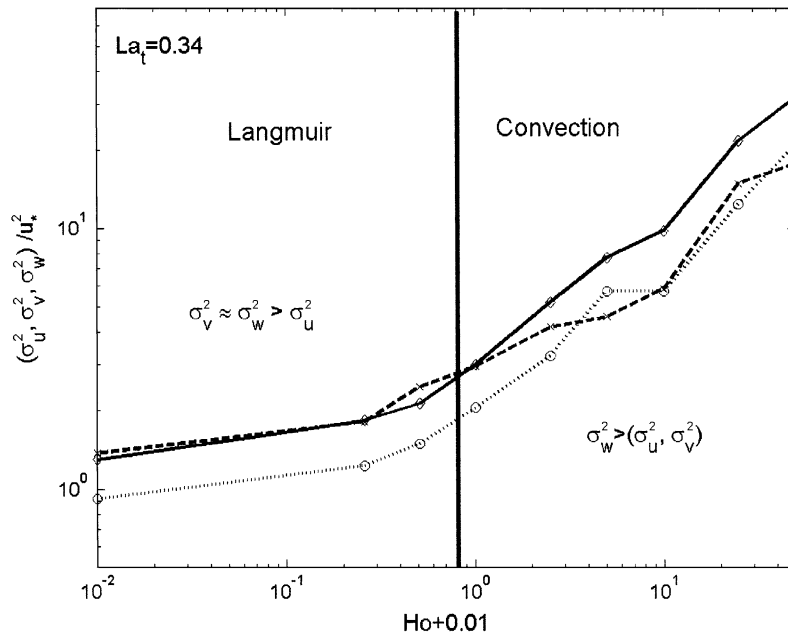


Fig. 8. Depth-averaged turbulent velocity variances (solid for vertical component, dashed for crosswind and dotted for downwind component) as functions of Ho at $La_t = 0.34$, showing a transition from Langmuir to convective turbulence. The vertical line indicates $Ho_c \approx 0.8$ at which buoyancy and wind/wave forces contribute equally to the vertical turbulence intensity. To the left of this dividing line, turbulence intensities have an ordering of $\sigma_v^2 \approx \sigma_w^2 > \sigma_u^2$ characteristic of Langmuir turbulence. To the right of this line, they have an ordering of $\sigma_w^2 > (\sigma_u^2, \sigma_v^2)$ characteristic of convective turbulence.

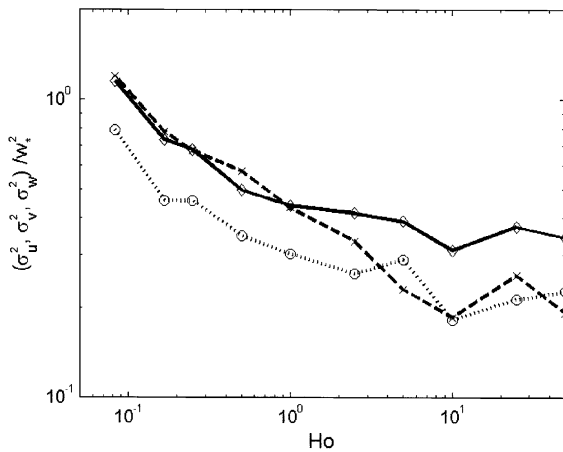


Fig. 9. Depth-averaged turbulent velocity variances scaled by the convective velocity scale. The solid line is the vertical component, the dashed line the crosswind and the dotted the downwind component.

One quantity of interest concerns the horizontal temperature anomaly which is often observed at the ocean surface. Convergent and divergent flows

in Langmuir turbulence produce warm or cool temperature anomalies at the surface. When the ocean is losing heat to the atmosphere, cool anomalies appear at the convergence zones (downwelling sites), whereas warm anomalies appear at divergence zones (upwelling sites). Combining scale analysis of boundary layer equations with 2D numerical results, LG95 obtained an empirical relation

$$\delta\theta \propto \frac{S_0\beta u_*}{\alpha g} La_t^{2/3} Ho \tag{14}$$

which suggests a linear relation between surface temperature anomalies and heat flux. To examine whether this simple relation holds up in more realistic 3D LES model, we calculate the root-mean square of temperature anomaly σ_θ at the ocean surface for a number of heating ($Ho < 0$) and cooling ($Ho > 0$) cases. As shown in Fig. 10, σ_θ indeed varies as a linear function of Ho and extends over a range ($-0.5 < Ho < 1$), although departure from the linear function is clearly visible

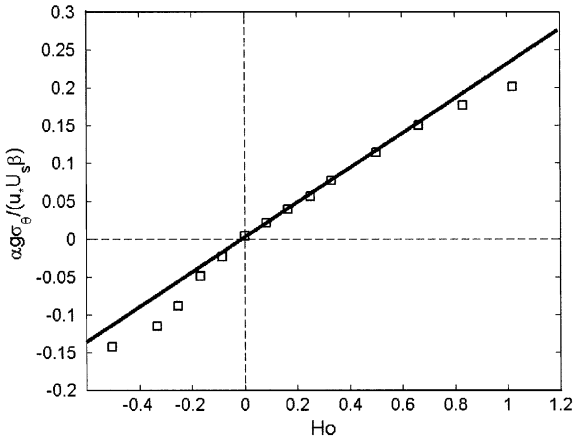


Fig. 10. Surface temperature anomaly as a function of Ho . Data points represented by square symbols are obtained from the LES model, while the solid line represents a linear approximation as suggested from previous 2D results. We assign positive (negative) values for the cooling (heating) cases.

in the heating case. With typical values of surface heat flux found over the ocean surface, the temperature anomalies obtained from the LES model are within a range of 0.02 K, in agreement with observed values (Thorpe and Hall, 1982; Farmer et al., 2001). Our runs have extended only to $Ho = -0.45$. Min and Noh (2004) find that Langmuir circulation is inhibited if $-Ho$ becomes larger than about 1 or 2.

Our standard model runs have a domain size of $120 \times 120 \times 50$ at 1 m resolution. To ascertain whether or not the results are sensitive to the domain size, we have conducted two comparative runs with a larger domain size of $160 \times 160 \times 50$ at 1 m resolution and $240 \times 240 \times 50$ at 2 m resolution. There is good agreement on turbulence fields in the upper part of the mixed layer, but differences are noticeable at lower depths. However, as shown in Fig. 11, low-order turbulence statistics converge between the three LES runs, although the coarse-resolution (2 m) run appears to have a difficulty in simulating weaker eddies at lower depths. Overall, the results on lower-order turbulence statistics are robust and are not sensitive to the choice of model resolution and domain size.

We have examined the transition from Langmuir to convective turbulence at $La_t = 0.34$. At

large values of La_t , turbulence has the characteristics of shear-driven turbulence. How will the addition of buoyancy forcing modify the dynamics of shear turbulence? Moeng and Sullivan (1994) compared shear- and buoyancy-driven turbulence in the atmospheric boundary layer. In this boundary layer, the geostrophic wind decreases to zero at the bottom boundary by frictional processes. In the ocean surface mixed layer, on the other hand, the flow is driven by wind stress at the surface. To examine whether Moeng and Sullivan's results apply to the ocean mixed layer, we have investigated the transition from shear to convective turbulence at $La_t = \infty$. In this limit Ho is no longer an appropriate dimensionless parameter to describe the comparison between the buoyancy force and shear force. Instead, we use the well-known ratio

$$\frac{H}{L} = -\frac{\kappa}{4}(\beta H)HoLa_t^{-2}, \quad (15)$$

where H is the mixed-layer depth, $L = -u_*^3/(\kappa B_0)$ the Monin–Obukhov length and κ is the von Karman constant (see LG95). H/L has been used as a bulk stability parameter, indicating the importance of convective instability of the mixed layer when the parameter is large and negative. Moeng and Sullivan (1994) found that the transition from shear to convective turbulence occurs around $H/(-L) = 4.5$ in the atmospheric boundary layer. Fig. 12a shows the vertical profile of the normalized vertical turbulence intensity at $(H/(-L)) = 0, 2.3$ and 9.3. It changes from the surface-intensified shape in the shear turbulence to a parabolic shape with a mid-depth maximum in the convective turbulence. The depth-averaged $\overline{\sigma_w^2}/u_*^2$ increases with increasing $H/(-L)$ and a quadrupling of $\overline{\sigma_w^2}/u_*^2$ (a doubling of rms vertical velocity) occurs around $H/(-L) = 4.5$, in agreement with that obtained by Moeng and Sullivan (1994).

5. The regime diagram and interpretation of turbulent kinetic energy equations

To cover the two-dimensional La_t-Ho parameter space, we have done a total of about 100 LES runs. When designing the model inputs, we

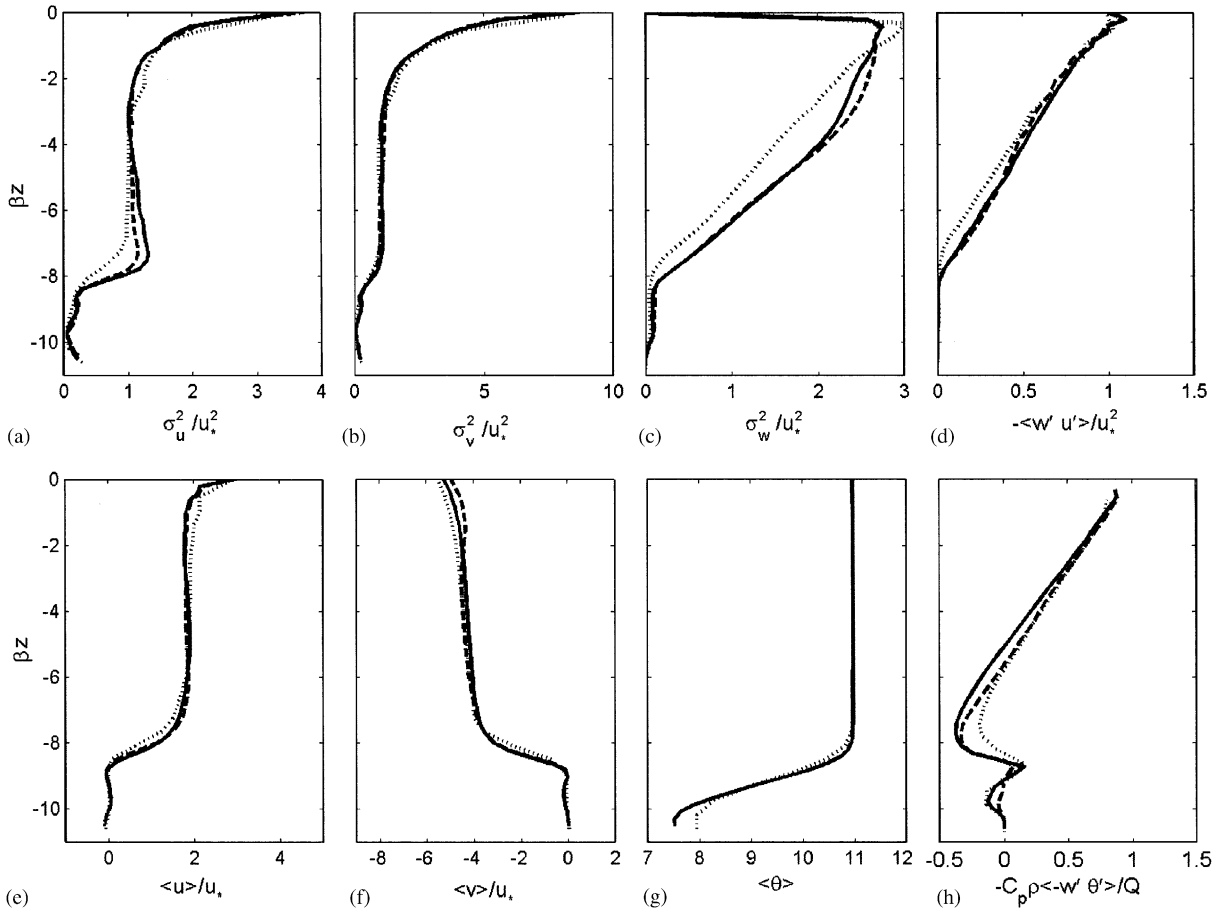


Fig. 11. Comparison of turbulence statistics at $La_t = 0.34$ and $Ho = 0.083$ but for three different combinations of model resolution and domain size. Solid lines represent a model domain of $160 \times 160 \times 50$ at 1 m resolution, dashed lines a model domain of $120 \times 120 \times 50$ at 1 m resolution, and dotted lines a model domain of $240 \times 240 \times 50$ at 2 m resolution. Vertical profiles of velocity variance in downwind (a), crosswind (b) and vertical (c) directions, momentum flux (d), mean velocity in downwind (e) and crosswind (f) directions, mean temperature (g) and heat flux (h).

vary the dimensional quantities over a broad range and sometimes use unrealistic values in order to cover all parts of the nondimensional parameter space. Wind speed ranges from 5 to 15 m s^{-1} , wave height from 0.2 to 4 m, surface heat fluxes from 0 to 1500 W m^{-2} of both positive and negative signs.

The depth-averaged vertical turbulence intensity $\overline{\sigma_w^2} / u_*^2$ is a key flow index to characterize turbulent flows in the ocean mixed layer. In Fig. 13 we show how it varies in the La_t – Ho parameter space. All transects along constant Ho lines show a trend similar to that at $Ho = 0$ (see Fig. 4). As La_t

increases, there is a rapid decrease in $\overline{\sigma_w^2} / u_*^2$ at small values of La_t but little change at large values of La_t . Transects along constant La_t lines show trends similar to that at $La_t = 0.34$ (see Fig. 8). Vertical turbulence intensity $\overline{\sigma_w^2} / u_*^2$ increases with increasing Ho . To display these regions more clearly, we have chosen a nonlinear scale in marking the contours. Fig. 13 suggests a division into three separate turbulence regimes. As one can see, there is little change in the flow index in the lower-right part of the parameter space. The vertical turbulence intensity can be solely scaled

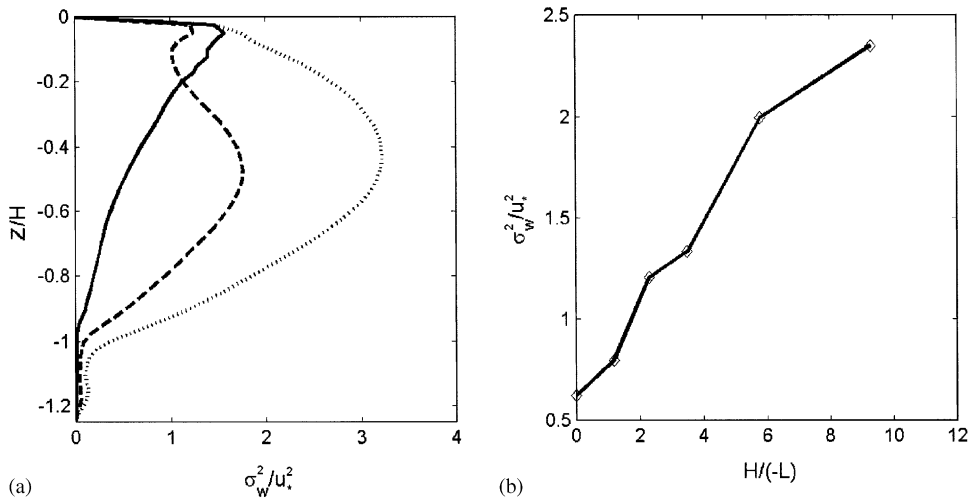


Fig. 12. Transition from shear to convective turbulence, (a) Vertical profiles of vertical velocity variances at three values of $H/(-L) = 0$ (solid), 2.3 (dashed) and 9.3 (dotted), (b) Depth-averaged vertical velocity variance as a function of $H/(-L)$.

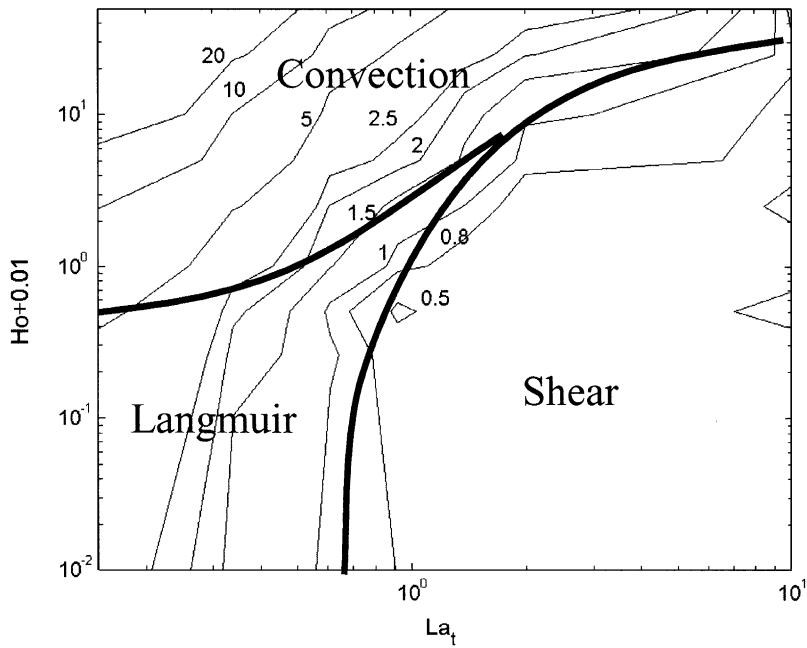


Fig. 13. Distribution of depth-averaged vertical velocity variance σ_w^2/u_*^2 in the La_t - Ho parameter space. The parameter space appears to be divided into three regions: a shear turbulence regime to the right, a Langmuir turbulence regime in the lower-left and a convective turbulence regime in the upper part. Note that a typical oceanic condition corresponds to $La_t = 0.3$ and $Ho = O(0.01)$.

by the friction velocity so that turbulence in this part of the parameter space is of shear type. Moving towards the left and upwards, we see a

steep gradient, which we have marked as a dividing line. Above that line, the vertical turbulence intensity changes at a fairly large rate. We

can divide the left domain into two sub-regions by selecting a line of Ho at which the vertical turbulence intensity doubles that at $Ho = 0$. This threshold value Ho_c increases with La_t and ranges from 0.5 to 5. The parameter space below that line can be named the Langmuir regime whereas the region above that line named the convective regime. For realistic oceanic values, one has $La_t = 0.3$ and $Ho = 0.01$. This would put a typical oceanic condition in the Langmuir regime. Of course, under cooling and low-wind conditions, Ho will be large and turbulence in the mixed layer will be in the convective regime.

The LES results have shown that turbulence in the ocean mixed layer is not isotropic. The degree and characteristics of anisotropy are different between convective, shear and Langmuir turbulence. To understand these differences, we examine the horizontally-averaged turbulence kinetic energy (TKE) equations for three velocity components. We assume that the turbulence has reached a quasi-equilibrium state and the time tendency terms can be neglected. The turbulence exchange between the two horizontal velocity components due to the Coriolis force is also neglected. Following MSM, we write down the TKE equations as follows:

$$\frac{\partial \overline{\frac{1}{2}u'^2}}{\partial t} = 0 = \underbrace{-\overline{u'w'}}_S \frac{\partial \bar{U}}{\partial z} + \underbrace{\frac{1}{\rho} \overline{p' \frac{\partial u'}{\partial x}}}_P - \underbrace{\frac{\partial}{\partial \mathbf{x}} \left(\frac{1}{2} \overline{u'^2 \mathbf{v}'} \right)}_T - \underbrace{\varepsilon_x}_D, \quad (16)$$

$$\frac{\partial \overline{\frac{1}{2}v'^2}}{\partial t} = 0 = \underbrace{u_s \overline{u' \frac{\partial w'}{\partial z}}}_W - \underbrace{\overline{v'w'}}_S \frac{\partial \bar{V}}{\partial z} + \underbrace{\frac{1}{\rho} \overline{p' \frac{\partial v'}{\partial y}}}_P - \underbrace{\frac{\partial}{\partial \mathbf{x}} \left(\frac{1}{2} \overline{v'^2 \mathbf{v}'} \right)}_T - \underbrace{\varepsilon_y}_D, \quad (17)$$

$$\frac{\partial \overline{\frac{1}{2}w'^2}}{\partial t} = 0 = \underbrace{\frac{-\overline{u'w'}}{W} \frac{\partial u_s}{\partial z} - u_s \overline{u' \frac{\partial w'}{\partial z}}}_W + \underbrace{\alpha g \overline{w' \theta'}}_B + \underbrace{\frac{1}{\rho} \overline{p' \frac{\partial w'}{\partial z}}}_P - \underbrace{\frac{1}{\rho} \overline{\frac{\partial w' p'}{\partial z}}}_P - \underbrace{\frac{\partial}{\partial \mathbf{x}} \left(\frac{1}{2} \overline{w'^2 \mathbf{v}'} \right)}_T - \underbrace{\varepsilon_z}_D. \quad (18)$$

In the above equations, S represents shear production, W Stokes production by surface waves, B buoyancy production, P pressure transport, T turbulence transport, and D energy dissipation (ε_x , ε_y , ε_z are energy dissipation in three directions). We denote turbulence production terms in the three equations as Prod_u , Prod_v

and Prod_w . Because the sum of pressure transport terms is equal to zero due to incompressibility, the pressure terms P exchange energy between components, without changing the total amount of energy. Similarly, turbulent transport terms T only redistribute the turbulence energy among the three velocity components. Hence the turbulence production terms in three directions are $\text{Prod}_u = S$, $\text{Prod}_v = W + S$ and $\text{Prod}_w = W + B$.

In shear-driven turbulence, shear production P injects turbulence kinetic energy into the downwind component, which is then redistributed to the other two components by pressure and turbulent transport terms (Tennekes and Lumley, 1972). There is no direct turbulence production in the crosswind and vertical directions. This is shown well in Fig. 14a for a parameter set of $La_t = 1.76$ and $Ho = 0$ (so $B = 0$), which falls into the shear regime as discussed in Section 3. Turbulence generation $\text{Prod}_u = S$ due to shear production in the wind direction far exceeds the production in the other two directions. Because of the Coriolis force, a mean current develops slowly in the crosswind direction. The shear in this mean current (S term in Eq. (17)) also contributes to turbulence production in the crosswind direction, but it is small. Turbulence production $\text{Prod}_w =$

$W + B$ is weak because Stokes forcing is weak and $B = 0$. In the shear turbulence, therefore, the downwind component has more energy than the other two components as it receives most of the production of turbulence kinetic energy. This explains an ordering of downwind > crosswind > vertical component in turbulence intensity.

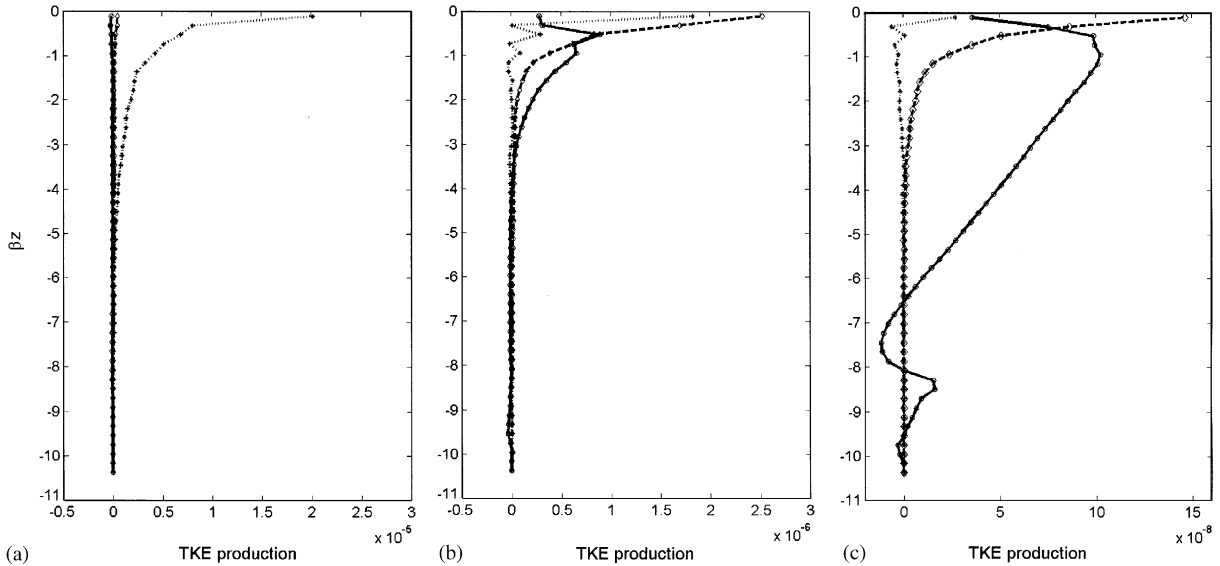


Fig. 14. Production of turbulent kinetic energy in the downwind (dotted), crosswind (dashed) and vertical (solid) directions for three representative LES runs: (a) $La_t = 1.76$ and $Ho = 0$ (shear turbulence); (b) $La_t = 0.34$ and $Ho = 0$ (Langmuir turbulence); (c) $La_t = 0.34$ and $Ho = 10$ (convective turbulence).

In contrast, for a parameter set of $La_t = 0.34$ and $Ho = 0$ in the Langmuir regime (Fig. 14b), Stokes production $Prod_v = W + S$ and $Prod_w = W + B$ (in which $B = 0$) directly generates turbulence kinetic energy in the crosswind and vertical directions. The Stokes production terms in the crosswind and vertical directions appear to have a similar magnitude, although they have different vertical profiles. These large turbulence production terms result in larger turbulence intensities in the crosswind and vertical directions. Moreover, the shear production in the downwind direction is much reduced (except very close to the sea surface) because the mean flow is homogenized. This explains smaller turbulence intensity in the downwind direction. Overall, the turbulence intensity has an ordering of crosswind \approx vertical > downwind in Langmuir turbulence.

In the buoyancy-driven turbulence, as shown in Fig. 14c for a parameter set of $La_t = 0.34$ and $Ho = 10$, buoyancy production $Prod_w$ is the largest component and generates turbulence energy in the vertical direction, although the Stokes production also contributes to turbulence production, as shown in the profile of $Prod_v$. Hence turbulence intensities in the convective regime

have an ordering of vertical > (downwind, crosswind) component.

6. Conclusions

Using a 3D LES model, we have investigated how buoyancy-driven thermal convection, wind-driven shear turbulence and wind/wave-driven Langmuir circulation compete to generate turbulence in the ocean surface mixed layer. We have examined the low-order turbulence statistics for a wide range of wind, wave and buoyancy forcing conditions and constructed a regime diagram to differentiate buoyancy-, shear- and wave-driven turbulence. In particular, we have studied changes of depth-averaged turbulence intensities in the La_t and Ho parameter space. All three types of turbulent flows are anisotropic but show different orderings of turbulence intensities in three directions: vertical > (downwind, crosswind) in convective turbulence; downwind > crosswind > vertical in shear turbulence; crosswind \approx vertical > downwind in Langmuir turbulence. These orderings of turbulence intensities can be explained by examining the turbulence energy production in three

directions. Buoyancy production in the vertical direction dominates turbulence generation in convective turbulence, whereas shear production in the downwind direction dominates turbulence generation in shear-driven turbulence. In Langmuir turbulence, however, Stokes production due to surface waves generates turbulence kinetic energy in both crosswind and vertical directions.

In the absence of air–sea heat flux, turbulence in the ocean surface mixed layer shows a rapid transition from shear to Langmuir turbulence as La_t decreases. In the shear regime the depth-averaged vertical turbulence intensity $\overline{\sigma_w^2}/u_*^2 \approx 0.7$ and is consistent with that obtained from a wall boundary layer. As La_t falls below 0.7, turbulence switches to Langmuir type and $\overline{\sigma_w^2}/u_*^2$ increases rapidly with decreasing La_t . A fully-developed sea state corresponds to $La_t \approx 0.3$ and lies within Langmuir regime. Normalized vertical turbulence intensity $\overline{\sigma_w^2}/u_*^2$ is about twice or larger than that in shear regime and falls into the range $\overline{\sigma_w^2}/u_*^2 = 1.35–3.0$ observed in the upper ocean. Hence, under typical sea state conditions, the wind-driven upper ocean will be dominated by Langmuir turbulence rather than shear turbulence. Although Langmuir circulation has previously been implicated as an important mixing mechanism, our model/data comparison has confirmed its dominant role in the upper ocean. Turbulence driven by wind stress alone is probably irrelevant to a wind-driven upper ocean unless surface waves are severely suppressed in extreme fetch-limited conditions. However, there will of course be shear-driven entrainment at the base of the mixed layer.

Previous study using a 2D model (LG95) suggested that Langmuir circulation dominates over thermal convection under typical atmospheric forcing conditions, say at wind speed at 10 m s^{-1} , surface heat loss rate of -200 W m^{-2} and fully-developed sea state. The current study using the 3D LES model confirms this result. We found that the transition from Langmuir to convective turbulence occurs around $Ho = O(1)$, which is much greater than $Ho = O(0.01)$ obtained using typical heat flux and wind speed values.

The regime diagram can be used to interpret upper-ocean turbulence observations. As we have shown in this paper, wind speed or surface heat

flux alone cannot determine the characteristic of turbulence in the mixed layer. What is important is the competition between the wind stress and the Stokes drift current and the competition between buoyancy forcing and wave forcing. When the wind speed, surface wave properties (directional wave spectrum) and air–sea heat fluxes are measured, we can calculate the values of dimensionless parameters La_t and Ho and locate the parameter pair in the regime diagram. This will help determine whether the upper ocean during the observational period falls into Langmuir, convective or shear regimes. As each of the turbulence types appears to have its unique characteristics, we may use existing analysis tools to diagnose and scale various turbulence quantities.

Although the model results can be used to guide the interpretations of observational data, we must caution that the LES model is only an approximation to the real upper ocean. For example, most of the air–sea momentum flux occurs through breaking waves, but it is parameterized here by a uniform wind stress at the sea surface. Surface waves in a real ocean consist of different frequencies and wave lengths. The associated Stokes drift current may have a profile different from the exponential profile and a vertical decay scale that changes in time. Although the precise shape of the Stokes-drift current profile is unlikely to be of first-order importance in deep mixed layers, it could be important in shallow mixed layers or in shallow-water lakes and inner shelf regions. In the LES model studied here, the Coriolis force causes the mean current to deflect to the right but does not significantly modify the dynamics of turbulent large eddies in the mixed layer. In a deep winter mixed layer, the Coriolis force will likely play a more important role so we may need to examine the effects of the Rossby number on the turbulence dynamics.

In this paper we did not investigate how pre-existing stratification affects turbulence dynamics in the upper ocean. This has simplified the analysis and condensed the dimension of the parameter space. A problem of critical importance to air–sea interaction is how these turbulent large eddies erode the stratification and redistribute water properties in the ocean surface boundary layer.

We are currently using the LES model to investigate how shear and Langmuir turbulence interact with a linearly stratified water and generate a surface mixed layer (see Li, 2004 for a preliminary report). We found that the mixed-layer deepening occurs through engulfment of stratified water in Langmuir turbulence but through localized Kelvin–Helmholtz billows in shear turbulence. The model results will be reported in a future paper.

Acknowledgements

We thank three anonymous referees for their insightful comments. This work is supported by a Grant (N000 14-02-1-0659) from the Office of Naval Research. This is UMCES contribution number 3798.

References

- D'Asaro, E.A., 2001. Turbulent vertical kinetic energy in the ocean mixed layer. *Journal of Physical Oceanography* 31, 3530–3537.
- D'Asaro, E.A., Dairiki, G.T., 1997. Turbulent intensity measurements in a wind driven mixed layer. *Journal of Physical Oceanography* 27, 2009–2022.
- Farmer, D.M., Vagle, S., Li, M., 2001. Bubble and temperature fields in Langmuir circulation. In: Lumley, J.L. (Ed.), *Fluid Mechanics and the Environment: Dynamical Approaches*, pp. 91–105.
- Huang, N.E., 1971. Deviation of Stokes drift for a deep-water random gravity wave field. *Deep-Sea Research* 18, 255–259.
- Kenyon, K.E., 1969. Stokes drift for random gravity waves. *Journal of Geophysical Research* 91, 191–208.
- Langmuir, I., 1938. Surface motion of water induced by wind. *Science* 87, 119–123.
- Li, M., 2004. Deepening of the ocean mixed layer by Langmuir and shear turbulence. *Proceedings of American Meteorological Society 16th Symposium on Boundary Layer Turbulence*. 11.10, 5 pp.
- Li, M., Garrett, C., 1993. Cell merging and the jet/downwelling ratio in Langmuir circulation. *Journal of Marine Research* 51, 737–769.
- Li, M., Garrett, C., 1995. Is Langmuir circulation driven by surface waves or surface cooling? *Journal of Physical Oceanography* 25, 64–76.
- Li, M., Garrett, C., 1997. Mixed-layer deepening due to Langmuir circulation. *Journal of Physical Oceanography* 27, 121–132.
- Lombardo, C.P., Gregg, M.C., 1989. Similarity scaling of viscous and thermal dissipation in a convecting surface boundary layer. *Journal of Geophysical Research* 94 (C5), 6273–6284.
- McWilliams, J.C., Sullivan, P.P., 2001. Vertical mixing of Langmuir circulations. *Spill and Science Technology* 6, 225–238.
- McWilliams, J.C., Sullivan, P.P., Moeng, C.-H., 1997. Langmuir turbulence in the ocean. *Journal of Fluid Mechanics* 334, 1–30.
- Min, H.S., Noh, Y., 2004. Influence of the surface heating on Langmuir circulation. *Journal of Oceanography*, in press.
- Moeng, C.H., Sullivan, P.P., 1994. A comparison between shear- and buoyancy-driven planetary boundary layer flows. *Journal of Atmospheric Science* 51, 999–1002.
- Noh, Y., Min, H.S., Raasch, S., 2004. Large eddy simulation of the ocean mixed layer: the effects of wave breaking and Langmuir circulation. *Journal of Physical Oceanography* 34, 720–735.
- Skylingstad, E.D., 2001. Scales of Langmuir circulation generated using a large-eddy simulation model. *Spill and Science Technology* 6, 239–246.
- Skylingstad, E.D., Denbo, D.W., 1995. An ocean large-eddy simulation of Langmuir circulations and convection in the surface mixed layer. *Journal of Geophysical Research* 100, 8501–8522.
- Skylingstad, E.D., Smyth, W.D., Moum, J.N., Wijesekera, H., 1999. Upper-ocean turbulence during a westerly wind burst: a comparison of large-eddy simulation results and microstructure measurements. *Journal of Physical Oceanography* 29, 5–28.
- Skylingstad, E.D., Smyth, W.D., Crawford, G., 2000. Resonant wind-driven mixing in the ocean boundary layer. *Journal of Physical Oceanography* 30, 1866–1890.
- Smyth, W.D., Skylingstad, E.D., Crawford, G.B., Wijesekera, H., 2002. Nonlocal fluxes and Stokes drift effects in the K-profile parameterization. *Ocean Dynamics* 52 (3), 105–115.
- Tennekes, H., Lumley, J.L., 1972. *A First Course in Turbulence*. MIT Press, Cambridge, MA, 295pp.
- Thorpe, S.A., Hall, A.J., 1982. Observations of thermal structure of Langmuir circulation. *Journal of Fluid Mechanics* 114, 237–250.
- Weller, R.A., Price, J.F., 1988. Langmuir circulation within the oceanic mixed layer. *Deep-Sea Research* 35, 711–747.